M. HDDCC

CONF-760935 - P 3

Proceedings of the Second Topical Meeting on

The Technology of Controlled Nuclear Fusion

Volume III

September 21-23, 1976 Richland, Washington

Sponsored by

Richland Section and Controlled Nuclear Fusion
Division of American Nuclear Society
Electric Power Research Institute
and U.S. Energy Research and
Development Administration

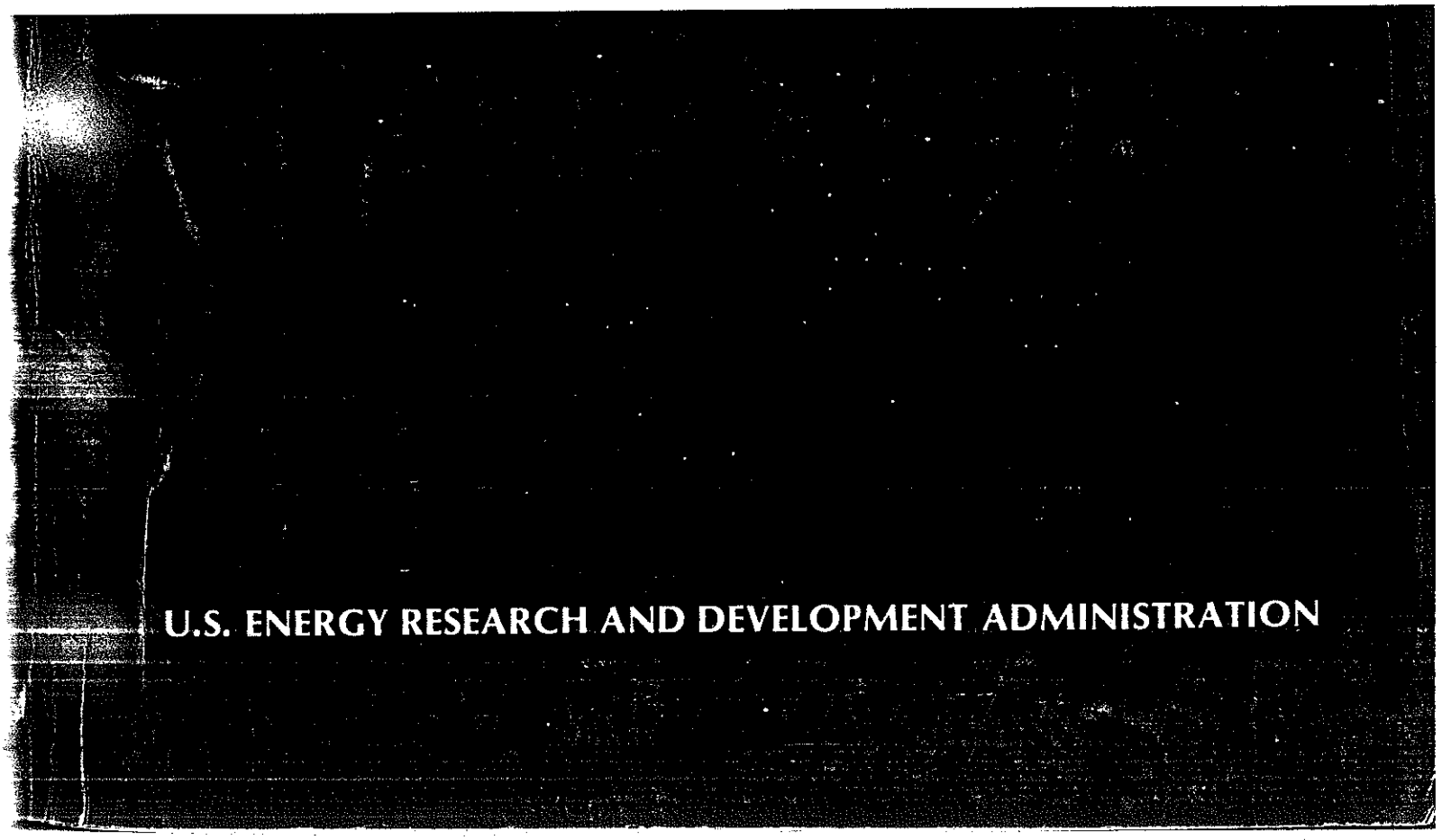

MULTIDIMENSIONAL NEUTRONICS ANALYSIS OF MAJOR PENETRATIONS IN TOKAMAKS*

M. A. Abdou, L. J. Milton, J. C. Jung, and E. M. Gelbard
ARGONNE NATIONAL LABORATORY, ARGONNE, ILLINOIS 60439

The blanket/shield system in tokamaks must provide for large size penetrations that can cause substantial streaming of nuclear radiation. Multidimenional neutronics calculations are used to examine the gross effects of major penetrations and their special shielding requirements. The study shows that it is feasible to shield against the effects of penetrations. However, the special shields for evacuation, neutral beam, and radio-frequency ducts occupy a substantial fraction of the reactor interior and their cost represents a significant cost item.

I. INTRODUCTION

The blanket/shield system in a Tokamak Experimental Power Reactor[1-4] (EPR), and in future tokamak fusion reactors as well, is required to accommodate a variety of penetrations including those for vacuum pumping, neutral beam and/or radio frequency (rf) heating, and experimental and maintenance access. These penetrations occupy typically ∿5-10% of the blanket/shield volume. Penetrations such as those for vacuum pumping and neutral beam heating represent large void regions (∿0.5-1 m^2 in cross-sectional area) which extend from the first wall (directly visible to the plasma neutrons), radially through the blanket/shield, and on out between the toroidal-field (TF) coils. The functional requirements of the neutral beam ducts exclude any possibility of introducing any significant bends in the duct. Sharp bends in the evacuation ducts greatly reduce the efficiency of vacuum pumping and they force the designer to increase the size of the ducts.

The need to guard against the potential problems that can be created by radiation streaming assisted by the presence of these penetrations, is obvious. The blanket/shield system provides, in general, about six orders of magnitude attenuation of nuclear radiation in order to protect the TF coils and auxiliary systems located on the exterior of these coils from excessive radiation damage, nuclear heating, and induced activation. The volume fraction of the major penetrations indicate that these penetrations would cause more than 1% of the neutrons to escape into the exterior of the primary (bulk) shield. Thus the additional special penetration shield will have to provide roughly four orders of magnitude of attenuation for neutrons streaming in the presence of penetrations. Therefore, the special shields for penetrations represent a very significant part of the shielding system in EPR and are expected to remain equally important in future tokamak reactors. The design of a penetration shield is more difficult, however, than the design of the primary bulk shield in two respects: (1) treatment of penetrations requires three-dimensional neutronics analysis; and (2) the geometry of the reactor imposes severe restrictions on the availability of space for penetration

*Work supported by the U. S. Energy Research and Development Administration.

shields, above and beyond the space restrictions on the bulk shield. Moreover, as will be shown later in this paper, the neutral beam ducts can be shielded on the sides only. Thus, there is always a straight-through path for the neutrons, a path leading to the beam injector and onto the exterior of the reactor.

The penetrations in a tokamak reactor can be classified, in general, into two types: (1) major penetrations; and (2) normal penetrations. The major penetrations are those penetrations that are large in size and their functional requirements do not permit substantial modifications in their shape. These major penetrations include, for example, the evacuation, neutral beam, and rf ducts. On the other hand, the normal penetrations are small and are ameanable to substantial shaping of their path inside the blanket/shield. Among the penetrations in this category are, for example, the coolant channels, clearances between shield blocks, and some of the small penetrations for diagnostics. This classification is of great importance with respect to the development of a strategic procedure for the design of a reactor. The effects of normal penetrations can be regarded as moderate perturbations on the performance of the system. Thus, although the impact of these normal penetrations should be anticipated qualitatively in the early stages of the design, their detailed design and analysis can be deferred until later stages of the overall reactor design process without much penalty. On the other hand, the effects of the major penetrations and their special shields on many of the reactor components is so great that these effects must be factored into the design as early as possible. By treating the major penetrations and their special shields as an integral part of the reactor system, many of the tradeoffs and conflicts can be resolved at early stages of the design. This paper presents some results of a neutronics study on the effects of major penetrations in tokamaks and analysis of their special shield requirements. More detailed information is given in Refs. 3 and 4.

II. CALCULATIONAL MODEL

Any penetration analysis depends to a great extent on many specific details of the reactor geometry and characteristics. The preliminary reference design for EPR documented in Refs. 1 and 2 was used for the initial parts of the penetration scoping study. This reference design has a major radius, R, of 625 cm and a circular plasma cross section with a minor radius, a, of 210 cm. There are 16 TF coils; each has a D-shaped vertical cross section with a horizontal bore of 7.7 m and a vertical bore of 11 m. A horizontal cross section of a TF coil is 0.60 m thick and 0.90 m wide. The blanket and primary shield consist of alternating zones of stainless steel (SS) and boron carbide (B_4C). A small segment of the blanket/shield at the inner side of the torus is 1.0 m thick while the rest of the blanket/shield is 1.31 m thick. In the reference design, as in any tokamak reactor, the inner segment of the blanket/shield cannot be utilized for placement of any major penetrations. These are generally accommodated on the top, bottom, and outer side of the torus. Therefore, the specific details of the inner segment of the blanket/shield will be ignored for the purpose of this work, and the blanket/shield is assumed to surround the plasma with a uniform thickness of 1.31 m. The inner radius of the first wall is 2.40 m. There are 32 vacuum ducts in the design, and each is cylindrical with an 0.85 m diameter. Two vacuum ducts are located at the top and bottom of the torus, equally spaced between each pair of the TF magnets. A cylindrical neutral beam duct with an 0.85 m diameter is located between each pair of TF magnets,

centered around the midplane, and its axis is nearly tangential to the toroidal magnetic axis.

The neutronics analyses were carried out using a three-dimensional geometric model with the continuous energy Monte Carlo Code VIM[5] and nuclear data from ENDF/B-IV.[6] Three-dimensional geometries are best treated at present with the Monte Carlo method. These calculations are inherently machine- and man-time consuming, making a thorough three-dimensional analysis of the full reactor geometry very costly. Therefore, a somewhat simplified three-dimensional geometric model, which is less costly but incorporates the basic features of the reactor geometry and accounts for all first-order effects of penetrations, was developed as described in detail in Ref. 3.

Figure 1 shows a schematic of the geometric representation for analysis of the vacuum ducts and their shields. If the toroidal magnetic axis is assumed to be a straight line, then Fig. 1 represents a cross section in the x-z plane where the z-axis is taken along the toroidal magnetic axis and the x-axis is parallel to the poloidal axis and passes through the plasma centerline. The system is symmetric around the midplane. A cross-section view in the x-y plane would show the blanket and the bulk shield as a set of concentric circles surrounding the circular plasma and scrape-off regions with one cylindrical vacuum duct at the top and another at the bottom. Figure 2 shows a schematic of the geometric representation for the analysis of the neutral beam ducts and their shields. A set of orthogonal coordinate systems (x,y,z) is also used here. The z-axis, as in Fig. 1, represents the toroidal magnetic axis, but the x-axis in the midplane and the y-axis is parallel to the poloidal axis. The axis of the beam duct is in the midplane (x-z plane) and makes an angle θ_b with the x-axis. Note that in both Figs. 1

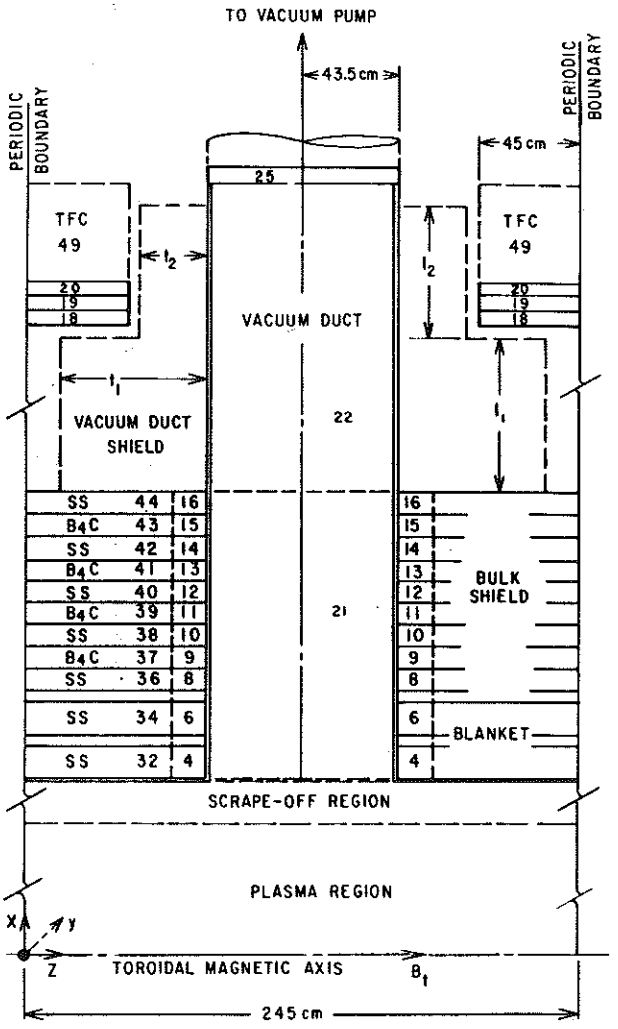

FIGURE 1. Schematic of Geometrical Representation for Analysis of Vacuum Ducts and Their Shields

and 2 the minor radius, r, for a point, is simply $r = \sqrt{x^2 + y^2}$.

In Figs. 1 and 2 some spatial zones are indentified by numbers that will be useful in later discussions. Zone 1 represents the plasma region and Zone 2 the scrape-off region. Zones 3-16 and 31-44 constitute the blanket-bulk shield. The wall of the penetration duct is represented as 1 cm thick tube of stainless steel that extends from the first wall to the exterior of the TF coils. The portion of the penetration duct inside the blanket and bulk shield is defined as Zone 21 and the corresponding portion of the duct wall is Zone 23. The

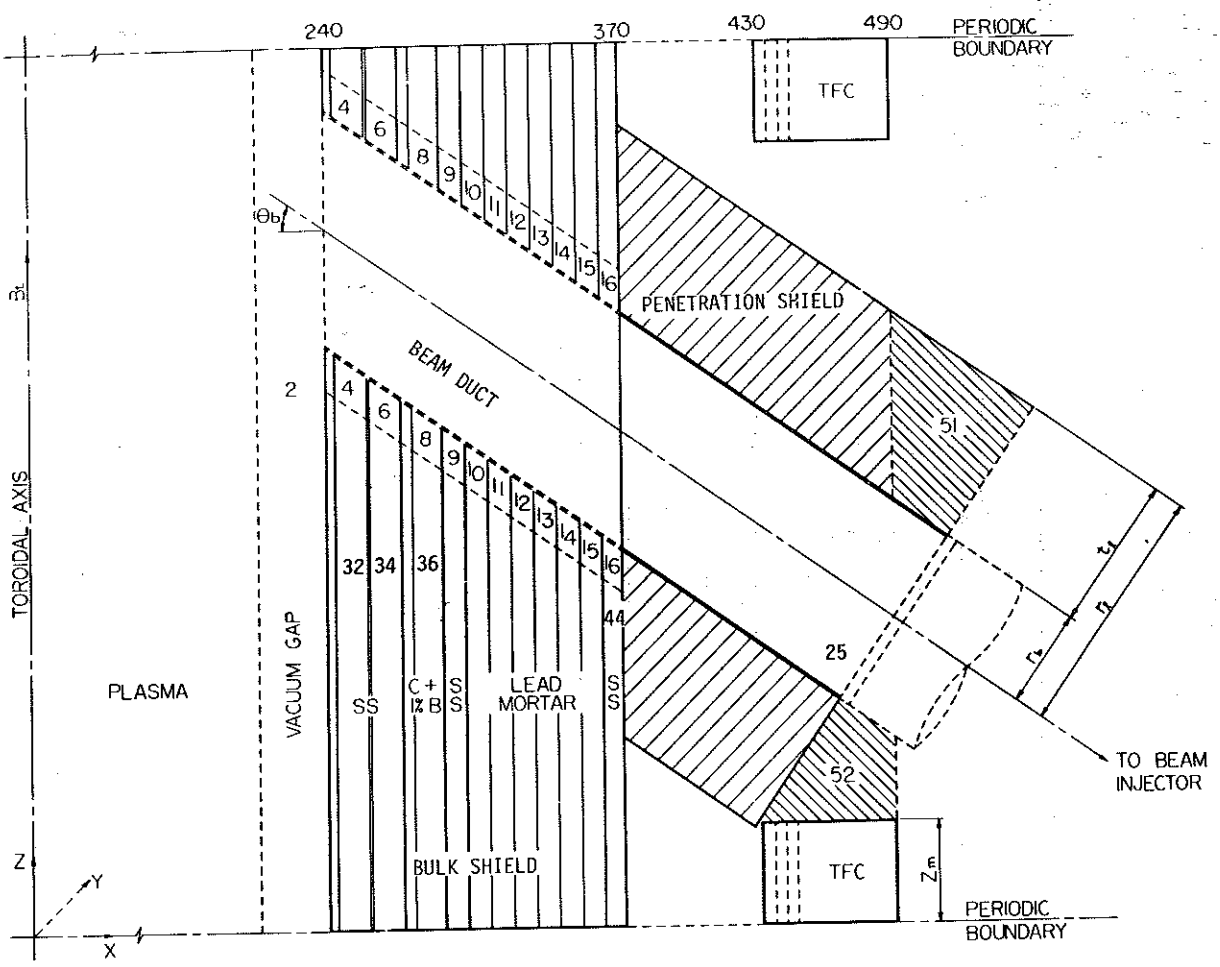

FIGURE 2. Schematic of Geometry Representation for Analysis of Neutral Beam Penetrations and Their Shields

part of the penetration duct outside the blanket-bulk shield is Zone 22 and the corresponding portion of the duct wall is Zone 24. The neutral beam and evacuation duct extend far beyond the TF coils in a detailed design. A neutral beam duct generally extends ∿2.5 m beyond the TF coils and leads to the large size chamber of the beam injector. Many components are located inside the beam injector, such as the neutralizer, bending magnets, cryosorption panels, ion source, and accelerator. An evacuation duct leads to a vacuum pump. An evacuation duct can be bent before it is connected to a vacuum pump, but at the expense of a reduction in the pumping efficiency. If the vertical bore of the magnet is large enough, the vacuum duct can be bent external to the bulk shield and before it reaches the TF coils. In order to quantify the level of radiation streaming into the beam injectors and vacuum pumps, a 5 cm thick stainless steel disc was placed as an "end cap" on the penetration duct and is shown as Zone 25 in Figs. 1 and 2. The TF coils composition is homogenized as 50% SS + 50% Cu. These coils are divided into poloidal concentric rings, each 5 cm thick (depth). Each ring is divided into two zones. One zone is bound between two planes located at y = -100 and y = +100 and the other zone constitutes the rest of the ring. The first 5 cm ring consists of Zones 18 and 28 and the second 5 cm ring consists of Zones 19 and 29 with Zones 18 and 19 as the regions closer to the penetration duct.

III. ANALYSIS OF UNSHIELDED PENETRATIONS

Calculations for seven design sets, A-G

were made. Each set examines one or more aspects of the penetrations and their shield. This section is devoted to an analysis of the unshielded penetrations. Although it is clear that special shielding has to be provided to counteract the penetration effects, this analysis of unshielded penetrations is useful in providing insight into the requirements of such special shielding. Various schemes for shielding the penetrations are examined in the next section.

Design Set A includes three cases (1, 2, and 3), all of which have no penetrations, i.e. the blanket-bulk shield is solid and continuous everywhere. The variable parameter here is the blanket-bulk shield thickness, which is 131, 111, and 91 cm for cases 1, 2, and 3, respectively. The blanket and bulk shield composition for case 1 is that shown in Fig. 1. Cases 2 and 3 are obtained by eliminating outer parts of the shield with the appropriate thickness. The innermost radius of the TF coils in all cases is 430 cm. Table 1 shows the total neutron fluxes (normalized to 1 MW/m^2 neutral wall loading) at several key locations and the neutron leakage per DT neutron. In Table 1 and other tables in this paper, the percentage values in parentheses after each flux or leakage value represent the statistical error (i.e. the standard deviation) as estimated by VIM. These results show that increasing the thickness of the bulk shield by 20 cm reduces the level of nuclear radiation at the TF coils by a factor of >15. The tolerable level of nuclear radiation at the TF coils is generally determined from a tradeoff study of the conflicting requirements of the various reactor components and an optimization procedure to minimize the overall cost of the reactor per unit power output.[2,7] One constraint that cannot be violated, however, is that the radiation level at the TF coils must not exceed a level that permits the components of the superconducting magnet to function properly without excessive radiation damage and nuclear energy deposition. The magnet protection criteria depend on the design of the magnet and the specific superconducting and stabilizing materials. The radiation levels of cases 1 and 3 cover the range of acceptable levels for tokamak reactor designs that are of practical interest at present.[2,7]

Design Set B consists of cases 4, 5, and 6 which are similar to designs 1, 2, and 3, respectively, except for incorporating a cylindrical penetration duct that is 0.85 m

TABLE 1. Neutron Fluxes Normalized to a Neutron Wall Loading of 1 MW/m^2 for Design Set A

Case No.:	1	2	3
Thickness of Bulk Shield, cm	131	111	91
Diameter of Penetration Duct	none	none	none
No. of Histories	20,000	16,000	16,000
ϕ_{18}	9.93(6) (±18%)	1.85(8) (±14%)	3.19(9) (±13%)
ϕ_{19}	7.28(6) (±18%)	1.23(8) (±15%)	2.20(9) (±14%)
ϕ_{28}	9.93(6) (±18%)	1.85(8) (±14%)	3.19(9) (±13%)
ϕ_{29}	7.28(6) (±18%)	1.23(8) (±15%)	2.20(9) (±14%)
ϕ_{25}	9.90(6) (±18%)	1.85(8) (±14%)	3.20(9) (±13%)
Neutron Leakage per DT Neutron	1.16(-7)(±14%)	1.91(-6)(±13%)	2.93(-5)(±11%)

in diameter, as shown in Fig. 1. Results for cases 4, 5, and 6 are shown in Table 2. Comparison of results in this table with results shown in Table 1 for Design Set A shows that:

(1) The presence of penetrations causes a strong spatial variation of the TF coil neutron fluxes in the poloidal direction (i.e. along the circumference of the D-shape). The ratio of the neutron flux in region 18, ϕ_{18}, to that in region 28, ϕ_{28}, is ∿12. The penetrations also cause large variations in the toroidal direction across the TF coils.

(2) The penetrations increase the neutron flux in the TF coils by several orders of magnitude.

(3) Increasing the bulk thickness of the blanket-bulk shield from 0.91 to 1.31 m reduces the neutron flux at the magnet by a factor of ∿300 in the absence of penetrations but by only a factor of ∿3 when penetrations are present.

(4) The large-size penetrations assist a greater number of neutrons at high energy to reach the TF coils. This causes the increase in the transmutation, atomic displacement, and nuclear heating rates at the TF coil due to the presence of penetrations to be generally higher than the increase in the total neutron flux.

(5) The neutron leakage per DT neutron in the presence of penetrations is ∿2-3%, while in the absence of penetrations it varies from 1.2×10^{-7} for the 1.31 m bulk shield to 3×10^{-5} for the 0.91 m bulk shield.

(6) The neutron flux at the end cap, Zone 25, is ∿1.2×10^{13} n/cm^2 sec. (For comparison, the neutron flux at the first wall is 7.6×10^{14}.) This means that auxiliary systems located at the end of the penetration duct receive a significantly high dose of radiation.

The large-size penetrations enable a large number of neutrons and photons to reach magnets in two ways: (1) by creating possible direct line-of-sight from the plasma region to the magnets; and (2) increasing the population of the neutrons and photons in the blanket/shield regions in the vicinity of the void penetration where they can travel into the magnets through short paths in the blanket/shield. This second effect, generally called penetration-assisted radiation streaming, becomes more dominant as the size of the void penetration is decreased and the line-of-sight streaming is reduced. Both direct and assisted streaming are sensitive to the size of penetration for a given reactor configuration, as shown next.

Table 3 shows the neutron fluxes and leakage for cases 7 and 8 compared with case 4 discussed above. The diameter of the cylindrical penetration is varied from 0.85 m in case 4 to 0.42 m in case 7, and to 0.20 m in case 8. The results in Table 3 show that the neutron fluxes at the TF coils are reduced by more than an order of magnitude when the cross section area of the void penetration is reduced by a factor of 4. From the very limited number of cases in Table 3, it can be tentatively concluded that the total neutron flux at the TF coils is roughly proportional to the square of the cross section area of the void penetration. Thus the neutron flux at the TF coils is approximately proportional to d^4, where d is the characteristic dimension of the penetration cross section (e.g. d is the diameter of a circular cross section or the side length of a square cross section). These correlations are brought up here only to demonstrate qualitatively the great dependence of radiation streaming on the size of penetrations. The geometry of the system and the shape of the penetration are also important. For example, a penetration with a rectangular cross section with one side much larger than the other side is likely to result in less radiation streaming than another penetration with the same cross

TABLE 2. Total Neutron Fluxes Normalized to a Neutron Wall Loading of 1 MW/m^2 for Design Set B

Case No.:	4	5	6
Thickness of Bulk Shield, cm	131	111	91
Diameter of Penetration Duct, cm	85	85	85
Orientation of Penetration	perpendicular[(a)]	perpendicular	perpendicular
Penetration Shield Composition	none	none	none
No. of Histories	20,000	10,000	10,000
ϕ_{18}	4.08(12) (±9%)	6.19(12) (±17%)	1.03(13) (±9%)
ϕ_{19}	2.67(12) (±11%)	4.13(12) (±19%)	7.77(12) (±8%)
ϕ_{28}	3.42(11) (±7%)	7.11(11) (±8%)	1.14(12) (±14%)
ϕ_{29}	1.90(11) (±11%)	4.00(11) (±13%)	6.84(11) (±16%)
ϕ_{21}	1.59(14) (±3%)	4.59(14) (±4%)	1.50(14) (±6%)
ϕ_{22}	2.22(13) (±6%)	2.16(13) (±11%)	2.37(13) (±8%)
ϕ_{23}	1.48(14) (±3%)	1.50(14) (±4%)	1.27(14) (±5%)
ϕ_{24}	1.63(13) (±8%)	1.47(13) (±10%)	1.83(13) (±9%)
ϕ_{25}	1.19(13) (±10%)	1.14(13) (±17%)	1.83(13) (±12%)
Neutron Leakage per DT Neutron	1.97(-2) (±6%)	2.54(-2) (±8%)	3.18(-2) (±8%)

(a) Axis of duct is perpendicular to the toroidal axis as shown in Fig. 1.

TABLE 3. Total Neutron Fluxes Normalized to a Neutron Wall Loading of 1 MW/m^2 for Design Set C.

Case No.:	4	7	8
Thickness of Bulk Shield, cm	131	131	131
Diameter of Penetration Duct, cm	85	42	20
Penetration Shield Composition	none	none	none
No. of Histories	20,000	20,000	50,000
ϕ_{18}	4.08(12) (±9%)	3.51(11) (±18%)	1.10(10) (±56%)
ϕ_{19}	2.67(12) (±11%)	1.85(11) (±25%)	8.04(9) (±70%)
ϕ_{28}	3.42(11) (±7%)	2.56(10) (±34%)	2.50(9) (±65%)
ϕ_{29}	1.90(11) (±11%)	1.86(10) (±32%)	2.03(9) (±79%)
ϕ_{21}	1.59(14) (±3%)	1.24(14) (±6%)	8.65(13) (±7%)
ϕ_{22}	2.22(13) (±6%)	6.18(12) (±24%)	7.62(11) (±65%)
ϕ_{23}	1.48(14) (±3%)	1.14(14) (±7%)	8.65(13) (±7%)
ϕ_{24}	1.63(13) (±8%)	3.61(12) (±27%)	5.16(11) (±64%)
ϕ_{25}	1.19(13) (±10%)	4.30(12) (±43%)	5.35(11) (±100%)
Neutron Leakage per DT Neutron	1.97(-2) (±6%)	1.181(-3) (±20%)	8.26(-5) (±45%)

section area but with a square or circular cross section. Both direct and assisted streaming are strongly dependent on the size and shape of the penetration.

Comparing ϕ_{23} as well as ϕ_{24} for the three cases in Table 3 shows that the neutron fluxes along the walls of the penetration vary also with the penetration size. The neutron fluxes in the portion of the duct walls inside the blanket-bulk shield increase by ~30% when the diameter of the duct is doubled. The variation in the neutron fluxes in the portion of the duct walls outside the blanket-bulk shield with the size of the duct is much more pronounced. These results indicate that the spatial variation in response rates such as gas production and nuclear heating along the duct walls depends on the size of penetration and is generally stronger for smaller-size penetrations.

IV. SHIELDING OF MAJOR PENETRATIONS

The effect of major void penetrations can be classified into two categories. The first category includes the effects on reactor components external to the bulk shield due to a dramatic enhancement of radiation streaming. The effects on the penetration walls and blanket-bulk shield in the vicinity of the penetrations are included in the second category. Effects in the first category can be guarded against by incorporating efficient penetration shields, as examined in this section.

There are several shielding schemes which might be used to protect reactor components external to the bulk shield from enhanced radiation streaming caused by large-size penetrations. These are:

(1) Movable Shield Plug -- If the functional requirements of a penetration permit that the penetration be closed during the plasma burn, then a shield plug can be moved at the beginning of each pulse to close completely the penetration region embedded in the bulk shield.

(2) Local Component Shield -- Reactor components affected by radiation can be surrounded by a shield capable of reducing the radiation level in the component to a tolerable level.

(3) Bulk Shield Extension -- The bulk shield can be extended into and in between the TF coils, and onto the outside as necessary.

(4) Local (Exterior) Penetration Shield -- Each penetration is surrounded as it emerges from the bulk shield by an appropriate local shield. This shield must suffice to reduce the radiation level at the TF coils and at all other auxiliary systems located in the reactor building to a permissible level.

Each of these shielding approaches has its own merits and disadvantages. The movable shield plug is the easiest to define in terms of nuclear requirements, since it needs to have the same dimensions as the penetration itself and it can be of a composition similar to that of the blanket-bulk shield. The most important advantage of the movable shield plug is that, in contrast to all other approaches, it completely eliminates the penetration effects and restores the effectiveness of the bulk shield. It also requires the smallest inventory of shielding materials of the four options. Whether a movable shield plug is less costly and is more favorable than the other shielding schemes has yet to be determined from detailed studies including engineering and reliability considerations. A movable shield plug weighs several thousands of kilograms for the size of penetration discussed in this work. It also requires incorporating mechanical and electrical components as well as automatic control system, all of which must have high quality performance. Moreover, failure of these components has to be anticipated and the consequences must be assessed and factored into the design.

There is a finite probability that the movable shield plug will fail to close the penetration before initiation of the plasma burn. In such situations, a significant number of neutrons and photons would stream through the penetration. Repair of a major failure in the shield plug would have to be made remotely and would involve a down-time period for the reactor. However, in view of many disadvantages associated with other shielding schemes, a movable shield plug has to be considered as a serious candidate for penetration shielding. A movable shield plug should be considered only, of course, for penetrations whose functional requirements permit that they can always be closed during the entire duration of the plasma burn. This immediately eliminates, for example, a movable shield plug as a viable approach for neutral beam ducts in beam-driven devices and for divertors.

This study does not find the movable shield plug to be a viable approach for the neutral beam ducts for several reasons. One specific reason for near-term devices up to and including the tokamak EPR is that these machines may have to be operated in a beam-driven mode, either to offset subignition confinement or to prolong burn pulses. In this case, the beam duct cannot be closed during the time of plasma burn. For future tokamaks beyond EPRs, the movable shield plug does not appear attractive for the neutral beam ducts for reasons that include the following:

(1) During the plasma heating phase, the neutral beam is injected for a finite period of time and the fusion power increases steadily. The total energy of the neutrons emitted during the beam injection phase depends on the characteristics of the design but it is generally significant. Thus, radiation streaming during the plasma heating phase when the shield plug cannot be used is very likely to be intolerable. The same problem arises when the beam is used to extend the burn pulse.

(2) The neutral beam ducts have to provide a straight-through path from the neutralizer to the plasma chamber. Thus, the mechanical movements of the shield plug to close the neutral beam duct will involve rotational as well as displacement movements. This will involve time delay in closing the beam duct with the plasma already in the ignition phase. Moreover, complicated patterns of movements for placing the shield plug inside the beam duct will magnify the risk of failure that will always be associated with periodic mechanical movements of massive weights on a short time scale.

The second approach for penetration shielding is local shielding of components that are affected by radiation. This approach can be easily rejected as the primary approach on the ground of the large volumes of reactor components that have to be shielded; it is, however, a useful supplemental shielding method for some small-size equipment that is overly sensitive to nuclear radiation. Simple extension of the bulk shield is not an efficient technique for reducing radiation levels.

The local penetration shield approach takes full advantage of the specific shapes of penetrations, and of the fact that the penetrations may be located relatively long distances apart. In this approach, each penetration is surrounded as it emerges from the bulk shield by local shielding. The shapes and compositions of the local shields can be carefully adjusted so as to conserve space and minimize cost. With this local penetration shield approach, the dimensions of the bulk shield, for a given material composition, should be no greater than the minimum required for the protection of the TF coils in regions far away from the penetrations (i.e. in the complete absence of any penetration effects). The local

penetration shield approach requires extensive nuclear analysis to determine the appropriate material composition and the optimum geometrical shape for each particular type of penetration. In this study, a modest attempt is made to examine the gross features of a local penetration shield.

Because of constraints on available space for local penetration shields it is important to find an effective shield material which is not unduly expensive. Such a composition was found in Refs. 2 and 7 for typical fusion reactor spectra to be a mixture of stainless steel and boron carbide. Design Set D in Table 4 allows for a penetration shield whose composition is 50% SS + 50% B_4C in case 9, all stainless steel in case 10, and all B_4C in case 11. The geometry of the system is as shown in Fig. 1, with the inner radius of the TF coils as 4.30 m. The penetration shield is 0.30 m thick and extends from the bulk shield to the end cap. The results in Table 4 show that the 50% SS + 50% B_4C penetration shield in case 9 gives much better overall attenuation than we find in cases 10 and 11. Comparing cases 9 and 11 shows that the 50% SS + 50% B_4C penetration shield lowers the radiation level at the TF coils and other components on the side of the shield by about a factor of 7 compared with the all-B_4C penetration shield. However, the radiation level in both cases is essentially the same at the open ends. The problem is just that — open ends. Some neutrons, travelling in the void duct, strike the penetration shield adjacent to the side of the duct, but others do not; many neutrons scatter from the side penetration shield into the duct where they can travel for a long path before they can make another collision on the side shield. Thus, the attenuation of neutron fluxes outward in the void duct will tend to be weak. This effect, as will be seen shortly, persists regardless of the thickness of the penetration shield.

Comparing case 9 in Table 4 with case 4 in Table 2 shows that the use of an 0.30 m thick penetration shield results in a factor of 40 reduction in the neutron fluxes at the TF coils. However, in reference to case 1 in Table 1, the penetration shield needs substantial improvement to provide an additional four orders of magnitude in attenuation in order to completely eliminate the penetration effects at the TF coils. Design Set E in Table 5 examines the effects of the penetration shield thickness and length. In cases 12, 13, and 14, only the first 15 cm of the magnet depth are included in the calculation in order to eliminate the computer time consumed in tracking particles traveling inside the TF coils (i.e. in region 49 in Fig. 1). Case 9 of Table 4 is also shown in Table 5 for comparison purposes. All penetration shields in cases 12, 13, 14, and 9 have a 50% SS + 50% B_4C composition. The penetration shield in case 12 is 0.30 m thick and covers only 0.55 m of the duct length external to the bulk shield. The penetration shield in case 13 has the same length as that of case 12 but is 0.75 m thick. The penetration shield in case 14 is 0.75 m thick in the region between the bulk shield and inner surface of the magnet then narrows down to fully occupy the 0.34 m thick region between the TF coils.

Results for cases 12 and 9 in Table 5 show that removing the portion of the penetration shield between the TF coils increase the neutron fluxes at the TF coil by a factor >2. Increasing the thickness of the penetration shield to 0.75 m without shielding the penetration segment which lies between the TF coils is an inefficient approach, as can be seen on comparing the TF coil fluxes for cases 13 and 9. The results in Table 5 show that increasing the thickness of the penetration shield from 0.30 m in case 9 to 0.75 m in case 14 (with the penetration covered from the outer surface of the bulk

TABLE 4. Total Neutron Fluxes Normalized to a Neutron Wall Loading of 1 MW/m^2 for Design Set D

Case No.:	9	10	11
Thickness of Bulk Shield, cm	131	131	131
Diameter of Penetration Duct, cm	85	85	85
Penetration Shield Composition	50% SS + 50% B_4C	SS	B_4C
Dimensions of Penetration Shield	$t_2 = t_1 = 30$ cm $\ell_1 + \ell_2 = 119$ cm	$t_2 = t_1 = 30$ cm $\ell_1 + \ell_2 = 119$ cm	$t_2 = t_1 = 30$ cm $\ell_1 + \ell_2 = 119$ cm
No. of Histories	30,000	10,000	10,000
ϕ_{18}	9.69(10) (±20%)	1.93(12) (±13%)	7.08(11) (±19%)
ϕ_{19}	6.04(10) (±23%)	1.27(12) (±23%)	3.30(11) (±20%)
ϕ_{28}	9.97(9) (±18%)	1.78(11) (±13%)	1.67(10) (±25%)
ϕ_{29}	7.37(9) (±22%)	1.14(11) (±21%)	1.67(10) (±27%)
ϕ_{21}	1.68(14) (±3%)	1.72(14) (±4%)	1.55(14) (±4%)
ϕ_{22}	3.37(13) (±5%)	4.53(13) (±8%)	2.32(13) (±8%)
ϕ_{23}	1.53(14) (±3%)	1.56(14) (±6%)	1.39(14) (±4%)
ϕ_{24}	2.88(13) (±5%)	-	-
ϕ_{25}	1.67(13) (±7%)	2.25(13) (±11%)	1.17(13) (±17%)
Neutron Leakage per DT Neutron	4.04(-3) (±7%)	1.10(-2) (±8%)	4.44(-3) (±12%)

TABLE 5. Total Neutron Fluxes Normalized to a Neutron Wall Loading of 1 MW/m^2 for Design Set E

Case No.:	12	13	14	9
Thickness of Bulk Shield, cm	131	131	131	131
Diameter of Penetration Duct	85	85	85	85
Penetration Shield Composition	50% SS + 50% B_4C	50% SS + 50% B_4C	50% SS + 50% B_4C	50% SS + 50% B_4C
Dimensions of Penetration Shield	$t_1 = 30$ cm $\ell_1 = 55$ cm $t_2 = \ell_2 = 0$	$t_1 = 75$ cm $\ell_1 = 55$ cm $t_2 = \ell_2 = 0$	$t_1 = 75$ cm $\ell_1 = 59$ cm $t_2 = 34$ cm $\ell_2 = 15$ cm	$t_1 = t_2 = 30$ cm $\ell_1 + \ell_2 = 119$ cm
No. of Histories	20,000	30,000	30,000	30,000
ϕ_{18}	2.17(11) (±21%)	1.31(11) (±12%)	1.32(9) (±79%)	9.69(10) (±20%)
ϕ_{19}	2.13(11) (±23%)	1.80(11) (±16%)	1.08(9) (±85%)	6.04(10) (±23%)
ϕ_{28}	2.11(10) (±26%)	4.84(8) (±41%)	2.44(6) (±100%)	9.97(9) (±18%)
ϕ_{29}	1.06(10) (±34%)	3.14(8) (±42%)	NS[a]	7.37(9) (±22%)
ϕ_{21}	1.58(14) (±4%)	1.52(14) (±3%)	1.58(14) (±2%)	1.68(14) (±3%)
ϕ_{22}	2.46(13) (±5%)	2.48(13) (±5%)	2.91(13) (±5%)	3.37(13) (±5%)
ϕ_{23}	1.44(14) (±4%)	1.38(14) (±3%)	1.41(14) (±3%)	1.53(14) (±3%)
ϕ_{24}	2.02(13) (±6%)	2.09(13) (±5%)	2.36(13) (±5%)	2.88(13) (±5%)
ϕ_{25}	1.23(13) (±10%)	1.14(13) (±8%)	1.28(13) (±7%)	1.67(13) (±7%)
Neutron Leakage per DT Neutron	9.60(-3) (±6%)	9.18(-3) (±6%)	8.80(-3) (±5%)	4.04(-3) (±7%)

(a) NS = no score = no neutrons reached this region in the histories run.

shield to in between the TF coils) reduces the neutron fluxes at the magnets by a factor of ∿70. There is an important difference between the penetration shields in cases 9 and 14 besides the different thickness. In case 9 the penetration shield covers the penetration fully, i.e. it extends to the end cap. In case 14, however, the penetration shield covers only those portions of the penetration which lie between the bulk shield and the TF coils, and extends in between the TF coils for only 0.15 m. Thus, the portion of the TF coils (0.15 m depth) included in the calculation is protected from direct line-of-sight exposure of any region inside the penetration duct in both cases. However, in case 14 the portion of the duct beyond the TF coils is left bare. This causes the neutron leakage in case 14 to be about twice that in case 9. A comparison of the neutron fluxes in zone 25, ϕ_{25}, and the neutron leakage for cases 9 and 14 reaffirms an important conclusion obtained earlier in this section. Regardless of how thick the penetration shield is made to be, extending the penetration shield to surround the portions of the void duct beyond the TF coils is necessary in order to protect auxiliary systems and equipment located external to the TF coils.

On comparing the results for cases 14 and 1, one sees that the attenuation obtainable with thick penetration shield in case 14 (0.75 m thick and tapered off to 0.34 m in between the TF coils) needs to be improved by an additional two orders of magnitudes in order to completely eliminate the penetration effects at the TF coils. Comparing the results of case 14 in Table 5 with Case 3 in Table 1 shows that if the magnet protection criteria are satisfied by the attenuation provided by the 0.91 m thick blanket-bulk shield in the absence of penetrations, then the penetration shield specified in case 14 is adequate to eliminate the penetration effects at the TF coils. Thus, the size of the penetration shield, as expected, depends strongly on the tolerable radiation level at the TF coils.

In cases 1 to 14 the width of the repeating segment, W_s, which is the distance along the z-axis between the two symmetry planes shown in Fig. 1 was taken as 2.45 m. The inner radius of the magnet, r_m, was taken in these cases to be 4.30 m. If the outer minor radius of the bulk shield is r_0, then the radial clearance, Δ_{sm}, between the bulk shield and the toroidal field coils is given as $\Delta_{sm} = r_m - r_0$. Obviously, the penetration effects and the design of the penetration shield should depend on W_s and Δ_{sm} in addition to the dependence on other parameters discussed earlier in this section and the previous section. The value of W_s depends on the major radius, the spacing between each pair of TF coils, and the coil width in the vicinity of penetration. For a given r_0, the value of Δ_{sm} depends on the actual shape of the toroidal-field coils, and on the location of the penetration. For a D-shaped TF coil, Δ_{sm} is larger on the top and bottom of the torus than on the outside at midplane. Conversely, W_s is smaller on the top and bottom of the torus than on the outside at midplane. This introduces a basic difference between the geometric representation of the evacuation ducts and that of the neutral beam ducts, in addition to the difference in orientation of the ducts. It will be recalled that the axis of the evacuation duct is perpendicular to the magnetic axis, while the neutral duct axis is almost tangential to the magnetic axis. In the following, the differences in the neutronics effects of the two types of penetrations are examined.

In the EPR design given in Ref. 1, and used for guidance in geometric representation of this penetration scoping study, each TF coil has a D-shaped vertical cross section with a horizontal bore of 7.7 m and a vertical

bore of 11 m. Thus, for the evacuation ducts located at the top and bottom of the torus, W_s = 2.45 m and Δ_{sm} = 1.79 m. Design Set F in Table 6 includes three cases: 15, 16, and 17 for the evacuation ducts. Case 15 is for unshielded evacuation duct. It should be noted that case 15 is similar to case 4 in Table 2 except that Δ_{sm} is 0.59 m in case 4 and 1.79 m in case 15. Comparing the results for these two cases shows that extending the vertical bore of the TF coils actually increases the neutron fluxes at the coils while the neutron leakage remains approximately the same. Case 16 in Table 6 incorporates a penetration shield that is 0.75 m thick and extends 0.60 m beyond the outer surface of the bulk shield. Thus case 16 is essentially the same as case 13 except that Δ_{sm} is 1.79 m in case 16 and 0.59 in case 13. Again, a larger number of neutrons can reach the TF coils when the magnet vertical bore is increased if the penetration shield is not extended to reach in between the coils. Case 17 in Table 6 is the same as case 16, except that the penetration shield length is increased from 0.60 m in case 16 to 1.0 m in case 17. This increase of 0.40 m in the penetration shield length reduces the neutron fluxes at the TF coils by only a factor of $\sim$2. Although the volume of the penetration shield in case 17 is more than 60% larger than that in case 14, the radiation level at the TF coils in case 17 is about a factor of 670 greater than that in case 14. This again is due to the fact that a portion of the evacuation duct near and in between the TF coils is left "bare" in case 17. A significant conclusion to be drawn, therefore, is that, for all practical purposes, increasing the bore of the TF coils cannot eliminate the need for effective shielding surrounding the evacuation duct in the regions where it passes between the TF coils. This is unfortunate since to make room for such a shield, it is necessary that the clearance space between a pair of TF coils be $\geq d + 2t_{ps}$, where d is the duct diameter and t_{ps} is the thickness of the penetration shield. To satisfy this requirement for a given major radius, d, t_{ps}, and TF coil width, the number of TF coils has to be reduced. The resulting increase in the magnetic field ripple then leads to enhancement of particle diffusion from the plasma. To avoid this situation, it seems that the vertical bore of the TF coils has to be increased, and the increase should be utilized in a different approach. If the increase in the magnet vertical bore is such that Δ_{sm} is significantly larger than $d + t_{ps}$ then the evacuation duct can be bent as it emerges from the bulk shield. Thus, the vacuum pumps can be moved so that they will no longer be visible to neutrons in the primary portion of the evacuation ducts, and at the same time both branches of the duct can be completely surrounded on all sides with penetration shield in order to protect the TF coils.

Cases 18 through 21 in Table 7 examine some of the neutronics aspects of the neutral beam ducts with the geometric representation shown in Fig. 2. The width of the repeating segment, W_s, in all these cases is 3.90 m, which leaves 3.0 m clearance between each pair of TF coils. The inner radius of the magnet, r_m, is 4.30 m in all cases. Cases 18 and 19 incorporate no penetration shield. In cases 19, 20, and 21 the axis of the beam duct makes a 55-deg angle with the toroidal magnetic axis, i.e., θ_b = 35° (see Fig. 2). For comparison, the axis of the beam duct in case 18 has a θ_b = 0°, i.e. this duct is perpendicular to the toroidal magnetic axis. Thus, case 18 is similar to case 4 except that W_s is 3.90 m in case 18 and 2.45 m in case 4. When the neutron fluxes in both cases are normalized to the same neutron wall loading, the results for the two cases provide a useful comparison

Table 6. Total Neutron Fluxes Normalized to a Neutron Wall Loading of 1 MW/m^2 for Design Set F

Case No.:	15	16	17
Thickness of Bulk Shield,[a,b] cm	131	131	131
Diameter of Penetration Duct, cm	85	85	85
Penetration Shield Composition	none	50% SS + 50% B_4C	50% SS + 50% B_4C
Dimensions of Penetration Shield	--	ℓ_1 = 60 cm	ℓ_1 = 100 cm
	--	t_1 = 75 cm	t_1 = 75 cm
	--	$\ell_2 = t_2 = 0$	$\ell_2 = t_2 = 0$
No. of Histories	20,000	20,000	20,000
ϕ_{18}	4.87(12) (±10%)	1.79(12) (±11%)	8.93(11) (±9%)
ϕ_{19}	3.61(12) (±10%)	1.31(12) (±15%)	5.61(11) (±12%)
ϕ_{28}	9.44(11) (±7%)	2.60(11) (±9%)	1.13(11) (±10%)
ϕ_{29}	6.12(11) (±6%)	1.44(11) (±9%)	6.86(10) (±11%)
ϕ_{21}	1.55(14) (±3%)	1.60(14) (±4%)	1.51(14) (±4%)
ϕ_{22}	1.58(13) (±7%)	1.62(13) (±7%)	1.90(13) (±7%)
ϕ_{23}	1.34(14) (±3%)	1.43(14) (±4%)	1.32(14) (±4%)
ϕ_{24}	1.12(13) (±6%)	1.23(13) (±7%)	1.48(13) (±7%)
ϕ_{25}	6.69(12) (±14%)	5.47(12) (±12%)	6.02(12) (±13%)
Neutron Leakage per DT Neutron	1.99(-2) (±5%)	8.94(-3) (±7%)	7.05(-3) (±8%)

(a) Blanket/shield composition is that shown in Fig. 1

(b) Basic geometry is as shown in Fig. 1.

(c) Basic geometry is as shown in Fig. 2.

TABLE 7. Total Neutron Fluxes Normalized to a Neutron Wall Loading of 1 MW/^{2} for Design Set G.

Case No.:	18	19	20	21
Thickness of Bulk Shield,[a,b] cm	131	131	131	131
Diameter of Penetration Duct, cm	85	85	85	85
Orientation of Penetration	θ_b = 0	θ_b = 35°	θ_b = 35°	θ_b = 35°
Penetration Shield Composition	none	none	50% SS + 50% B_4C	50% SS + 50% B_4C
Thickness of Penetration Shield	--	--	50 cm	70 cm
No. of Histories	20,000	20,000	40,000	40,000
ϕ_{18}	7.54(11) (±11%)	9.62(11) (±12%)	1.69(9) (±62%)	1.35(8) (±68%)
ϕ_{19}	5.97(11) (±13%)	5.83(11) (±16%)	2.06(9) (±67%)	3.41(8) (±65%)
ϕ_{28}	1.18(11) (±13%)	1.13(11) (±17%)	2.20(9) (±59%)	6.11(7) (±64%)
ϕ_{29}	7.30(10) (±17%)	7.78(10) (±18%)	9.20(7) (±75%)	3.43(7) (±79%)
ϕ_{25}	1.45(13) (±12%)	8.21(12) (±20%)	9.19(12)(±11%)	3.92(12) (±9%)
Neutron Leakage per DT Neutron	1.45(-2) (±6%)	9.45(-3) (±6%)	3.92(-3) (±6%)	4.00(-3) (±6%)

(a) Blanket/shield composition is that shown in Fig. 1.

(b) Basic geometry is as shown in Fig. 1.

(c) Basic geometry is as shown in Fig. 2.

between the effects of a penetration located at the top (or the bottom) of the torus and another that is located on the outside centered around the midplane. The neutron flux at the end cap, ϕ_{25}, is approximately the same in both cases (the difference is within the statistical uncertainty in the Monte Carlo calculations). Since the penetration size is the same in the two cases but W_s is substantially different, it can be concluded that the neutron flux inside the void penetration is fairly independent of the ratio of the void penetration volume to that of the blanket-bulk shield. The dependence on the penetration size was shown earlier in Section III to be very strong. Comparing ϕ_{18}, ϕ_{19}, ϕ_{28}, and ϕ_{29} for cases 4 and 18, one finds that the radiation level at the TF coils in case 18 is about a factor of 5 smaller than that in case 4. This means simply that increasing the clearance between the TF coils reduces the number of neutrons streaming into the TF coils. Thus, increasing the clearance between the TF coils should lead to an increase in the neutron leakage. When the neutron leakage per DT neutron is renormalized so that the DT neutron current at the first wall is the same in cases 4 and 18, the neutron leakage in case 18 is found to be indeed 30% higher than that in case 4.

With $\theta_b = 0°$ in case 18 and $\theta_b = 35°$ in case 19, the results for the two cases should provide an indication of the sensitivity of the neutronics effects of the beam duct to the orientation of the beam duct axis with respect to the magnetic axis. The differences in the neutron fluxes for the two cases as shown in Table 7 are found to be near the limits of the statistical uncertainty. Additional computation to reduce the statistical error was found unwarranted as these results already indicate that the neutronics effects of the beam ducts are not overly sensitive to the orientation of the beam axis with respect to the magnetic axis. There are many compensating and counteracting effects that tend to reduce the dependence on θ_b.

A penetration shield of 50% SS + 50% B_4C surrounds the beam duct in both cases 20 and 21 and extends from the outer bulk-shield boundary to the end cap. The beam duct shield is 0.50 m thick in case 20 and 0.70 m thick in case 21. The 0.50 m thick beam duct shield provides a factor of ∿570 reduction in the maximum neutron flux, ϕ_{18}, at the TF coils. The 0.70 m thick beam duct shield reduces ϕ_{18} by a factor of 12 relative to that with the 0.50 m thick shield. Comparing the results for case 21 with those for case 1 shows that the 0.70 m thick beam duct shield needs to be improved further in attenuation effectiveness by about a factor of 13 in order to reduce the maximum neutron flux at the TF coil to that in the absence of the beam duct. On the other hand, if the radiation level at the TF coils obtainable in case 2 is acceptable, then the 0.70 m thick beam duct shield is sufficient to protect the superconducting coils against radiation streaming caused by the neutral beam ducts. Note, however, that the neutron fluxes at the end cap and the neutron leakage obtainable with the 0.70 m thick beam duct shield are still very high. Thus, in order to protect other auxiliary systems located outside the TF coils, this beam duct shield should be extended (and tapered in proportion with the reduction in the radiation level) to the chambers of the beam injectors. Inside these chambers, the nuclear heating in the crysorption panel is ∿0.02 W/cm^3 for 1 MW/m^2 neutron wall loading and the absorbed dose in the bending magnet insulator is ∿10^{11} rad/(MW-yr/m^2).

The effects of radiation streaming on the nuclear performance of the walls of the neutral beam ducts and the blanket and shield regions in the vicinity of the ducts are found to be large. The neutron heating in

the water coolant at the inner edge (at the first wall) of the beam duct wall is ∿10 W/cm^3 and drops by less than a factor of 10 along the entire length of the beam wall inside the blanket-bulk shield. For comparison, the neutron heating drops along the same distance but in regions far removed from the ducts by a factor of 5×10^4. This strong redistribution of neutrons and secondary gammas requires that ∿20 cm thick region in the bulk shield surrounding the beam duct be provided with an efficient heat removal system similar to that employed in the blanket. In as much as the walls of the beam ducts must meet the same requirements as are imposed on the first wall, these duct walls pose potentially serious problems similar in magnitude and complexity to those imposed on the first wall.

While this study shows that it is feasible to shield against the effects of penetrations, the results also show that the special shields for the evacuation, neutral beam, and radio frequency ducts occupy a substantial fraction of the reactor interior and their cost represents a significant cost item.

REFERENCES

1. W. M. Stacey, Jr., et al., "Tokamak Experimental Power Reactor Studies," ANL/CTR-75-2, Argonne National Laboratory (1975).
2. M. A. Abdou"Nuclear Design of the Blanket/Shield System for a Tokamak Experimental Power Reactor," *Nucl. Technol.*, 29, 7 (1976).
3. W. M. Stacey, Jr., et al., "Tokamak Experimental Power Reactor Conceptual Design," ANL/CTR-76-3, Argonne National Laboratory (1976).
4. M. A. Abdou and J. Jung, "Nuclear Analysis of a Tokamak Experimental Power Reactor Conceptual Design," *Nucl. Technol.*, to be published.
5. E. M. Gelbard and R. E. Prael, "Monte Carlo Work at Argonne National Laboratory," in *Proc. NEACRP Meeting of a Monte Carlo Study Group*, ANL-75-2, Argonne National Laboratory (1974); also R. E. Prael and L. Milton, "A User's Manual for the Monte Carlo Code VIM," FRA-TM-84, Argonne National Laboratory (1976).
6. D. Garber, C. Dunford, and S. Pearlstein, "Data Formats and Procedures for the Evaluated Nuclear Data File, ENDF," BNL-NCS-50496 (ENDF-102), Brookhaven National Laboratory (1975); also TID-4500 (1975).
7. M. A. Abdou and C. W. Maynard, "Nuclear Design of the Magnet Shield for Fusion Reactors," in *Proc. 1st Topical Meeting on the Technology of Controlled Nuclear Fusion*, CONF-740402-P1 (1974), p. 685.